2020 IEEE/RSJ International Conference on Intelligent Robots and Systems (IROS)
October 25-29, 2020, Las Vegas, NV, USA (Virtual)

Robust Force Tracking Impedance Control of an Ultrasonic Motor-actuated End-effector in a Soft Environment

Wenyu Liang[1,*], Zhao Feng[2,*], Yan Wu[1], Junli Gao[3], Qinyuan Ren[4] and Tong Heng Lee[2]

Abstract— **Robotic systems are increasingly required not only to generate precise motions to complete their tasks but also to handle the interactions with the environment or human. Significantly, soft interaction brings great challenges on the force control due to the nonlinear, viscoelastic and inhomogeneous properties of the soft environment. In this paper, a robust impedance control scheme utilizing integral backstepping technology and integral terminal sliding mode control is proposed to achieve force tracking for an ultrasonic motor-actuated end-effector in a soft environment. In particular, the steady-state performance of the target impedance while in contact with soft environment is derived and analyzed with the nonlinear Hunt-Crossley model. Finally, the dynamic force tracking performance of the proposed control scheme is verified via several experiments.**

I. Introduction

Robotic systems have been increasingly used in many industrial and medical applications, where they are designed to work for various tasks under different environments. Significantly, many applications are required to carry out the contact operation between the end-effector and the environment or human, such as grasping, polishing, assembly [1], [2], microgripper [3], cell injection [4], surgery [5], and human-robot interaction [6], etc.

During the contact operation, the interaction force needs to be regulated carefully by force control to avoid undesirable effects (such as damage to environment) and ensure successful task performance [7], [8]. Various force feedback control schemes are presented in [9]–[11], which show good effectiveness of applying force controller in different applications. These explicit force controllers can achieve fast response and low force overshoot when the contact model is established accurately. However, it is noted that the motion of the actuation system is unconstrained and uncontrolled for pure force controllers.

Alternatively, the interaction force can be regulated by the target impedance model through establishing a virtual mass-spring-damper dynamics with contact force and position errors [12]. To track the desired interaction force trajectory, a force tracking impedance control was proposed in [13]. In [14], it is demonstrated that impedance control achieves better performances than explicit force control, especially for microscale applications. It is worth noting that the contact environment is generally assumed to be rigid and described by a simple elastic or mass-spring-damper system. The rigid environment can be suitable for the applications such as polishing [15], electro-hydraulic force loading system [16], microassembly [17]. However, for applications that the systems are required to be in contact with soft environment, e.g., human tissues to surgical devices, new challenges on force tracking arise because the soft environment is generally viscoelastic, nonlinear and inhomogeneous [18].

To describe the dynamics between the end-effector and the soft environment, many linear compliant contact models have been developed and used [8], [19]. Moreover, the experimental results reported in [18], [20] show that the soft materials such as human tissues/organs can be more accurately modeled by the Hunt-Crossley (HC) nonlinear model. Nevertheless, only few studies used this nonlinear model in the force controller design [21].

Another concern about force tracking in a soft environment is the robustness to unintended impacts stemmed from the environment and the end-effector. Many approaches have been developed to handle the robustness problems for position tracking [22]–[24]. Among these, sliding mode control (SMC) provides effective and robust performance by taking the undesired impacts as external disturbances. To regulate interaction force and remain sufficiently robust, a robust sliding mode impedance controller without knowing the exact values of system parameters is proposed in [25]. However, the finite-time convergence of SMC that are vital to tracking performance is not considered. Also, few studies explored on the impedance control in a soft environment.

In this paper, an ultrasonic motor-actuated (USM-actuated) end-effector is developed and used in investigating the robust impedance control for force tracking in a soft environment, where a thin soft membrane is employed to represent the soft environment. Apart from the soft environment, the inherent hysteresis nonlinearity and the produced friction in the USM can deteriorate the system performance significantly [26]–[28]. Motivated by these key issues, an integral backstepping impedance control with integral terminal sliding mode (BC-ITSMC) based on the HC model is proposed to achieve high force tracking precision and strong robustness to complex hysteresis and friction nonlinearities, disturbances, and varied properties of different soft environments.

This work is partially supported by the Agency for Science, Technology and Research (A*STAR) under its AME Programmatic Funding Scheme (Project #A18A2b0046).

*W. Liang and Z. Feng contributed equally to this work.

[1]W. Liang and Y. Wu are with the Institute for Infocomm Research (I^2R), Agency for Science, Technology and Research (A*STAR), Singapore 138632. (Liang_Wenyu@i2r.a-star.edu.sg and wuy@i2r.a-star.edu.sg)

[2]Z. Feng and T. H. Lee are with the Department of Electrical and Computer Engineering, National University of Singapore (NUS), Singapore 117576. (fengzhao@u.nus.edu and eleleeth@nus.edu.sg)

[3]J. Gao is with the School of Automation, Guangdong University of Technology, Guangzhou, China 510006. (jonygao621@gdut.edu.cn)

[4]Q. Ren is with the College of Control Science and Engineering, Zhejiang University, Hangzhou, China 310027. (renqinyuan@zju.edu.cn)

The rest of this paper is organized as follows. The end-effector and its model are introduced in Section II. The impedance model and steady-state error analysis in soft environment based on the HC model are presented in Section III. Section IV gives the detailed design of the proposed controller. Experimental setup and results are presented in Section V. Finally, Section VI draws the conclusions.

II. Ultrasonic Motor-Actuated End-Effector

The USM-actuated end-effector equipped on to a manipulator (KUKA LBR iiwa 14) is shown in Fig. 1, which is mainly designed for carrying out precise surgical operation (e.g., automatic injection and implant insertion [5]), as well as micromanipulation. There are two key components in the end-effector that make it functional, one is the USM (PI-M663, Physik Instrumente) with the resolution of 0.3 μm to move the tool and the other is a force sensor (FS1500NS, Honeywell) with the sensitivity of 0.12 mV/g to measure the interaction force between the tool and environment.

The USM is a piezoelectric actuator, which dominant part can be modeled as a second-order system [26]. With the consideration of the hysteresis, friction and other disturbances, the USM model is expressed as

$$m\ddot{x} + c\dot{x} + kx + f_c + f_h + f_d = bu - f_e, \tag{1}$$

where m, c, k are the effective mass, damping and stiffness coefficients, respectively. x is the measured position. $\dot{x}$ and $\ddot{x}$ are the velocity and acceleration, respectively. f_e is the measured interaction force between the device and environment. The input voltage to the USM is denoted as u through a electromechanical ratio b of the system. f_c and f_h are the friction and hysteresis nonlinearities, respectively, f_d is the unknown disturbances, e.g., heat and external disturbances.

A diagram showing the contact model between the USM-actuated end-effector and the environment is depicted in Fig. 2, where k_e, b_e and n are the parameters of the environment, and x_e is the equilibrium position of the environment.

Assumption 1. The time derivative of f_c, f_h, f_d are bounded and satisfy the following conditions: $|\dot{f}_c| \leq \Theta_c$, $|\dot{f}_h| \leq \Theta_h$, $|\dot{f}_d| \leq \Theta_d$, where Θ_c, Θ_h, Θ_d are positive constants.

Because the actual parameters of the system are difficult to obtain, the nominal parameters are defined as $m_n = m - \Delta m$, $c_n = c - \Delta c$, $k_n = k - \Delta k$, where Δm, Δc, Δk are the model uncertainties.

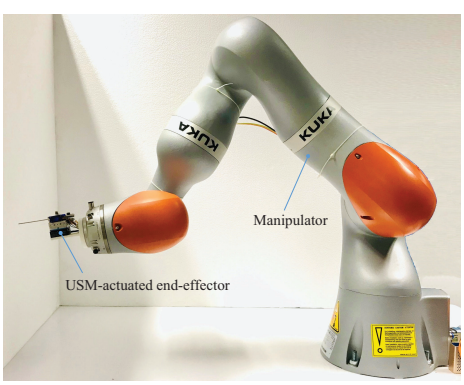

Fig. 1. USM-actuated end-effector with manipulator

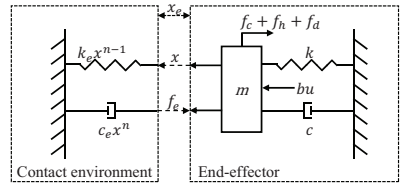

Fig. 2. Model of USM-actuated end-effector during contact

Assumption 2. The time derivative of the model uncertainties $\Xi = \Delta m\ddot{x} + \Delta c\dot{x} + \Delta kx$ are bounded by $|\dot{\Xi}| \leq \Theta_\Xi$, where Θ_Ξ is a positive constant.

The total disturbance is defined as $f_t = \Delta m\ddot{x} + \Delta c\dot{x} + \Delta kx + f_c + f_h + f_{ed}$ and its time derivative is bounded by $|\dot{f}_t| \leq \Theta_{f_t} = \Theta_\Xi + \Theta_c + \Theta_h + \Theta_d$, where Θ_{f_t} is an unknown positive constant.

Based on the above assumptions, (1) is simplified as

$$m_n\ddot{x} + c_n\dot{x} + k_n x + f_t = bu - f_e. \tag{2}$$

III. Impedance Model and Steady-State Error Analysis in Soft Environment

To regulate the position and force simultaneously, the initial impedance model is formulated in terms of the position error and interaction force [12]. However, for many applications such as robotic surgery and soft grasping, the force tracking is also required to achieve the desired response. Thus, the target impedance model including both position and force errors is employed in this paper, which is given by

$$m_i\ddot{e}_p + c_i\dot{e}_p + k_i e_p = -k_f e_f, \tag{3}$$

where m_i, c_i, k_i are the desired inertia, damping, stiffness impedance parameters, respectively. k_f is the parameter to regulate the weighting of force error. The term $e_p = x - \bar{x}$ is the position error, and $e_f = f_e - \bar{f}$ is the interaction force error, where $\bar{x}$ and $\bar{f}$ are the desired position and force trajectories, respectively. With the virtual mass-spring-damper relationship (3), the position and force can be controlled at the same time via selecting suitable impedance parameters.

As shown in Fig. 2, the HC nonlinear model used to describe the soft environment is expressed as

$$f_e = k_e(x - x_e)^n + c_e(x - x_e)^n\dot{x}, \tag{4}$$

where x_e is the equilibrium position of the environment in absence of interaction force. $k_e(x - x_e)^{n-1}$ and $c_e(x - x_e)^n$ are position-dependent stiffness and damping.

Take the HC model (4) into (3), we can obtain that

$$\begin{aligned} m_i\ddot{e}_p + c_i\dot{e}_p + k_i e_p = -k_f[&k_e(x - x_e)^n \\ &+ c_e(x - x_e)^n\dot{x} - \bar{f}]. \end{aligned} \tag{5}$$

It is clear that the equation is nonlinear and thus difficult to be solved. To analyze the steady-steady performance, the HC model is firstly linearized [21]. Assuming that the corresponding equilibrium position reaches at x_s for the

desired force $\bar{f}$, by employing Taylor series of x and $\dot{x}$ at x_s, we can derive the following approximation

$$\begin{aligned} f_e(x,\dot{x}) \approx & f_e(x_s,\dot{x}_s) + \left.\frac{\partial f_e}{\partial x}\right|_{x_s,\dot{x}_s} [(x-x_e)-(x_s-x_e)] \\ & + \left.\frac{\partial f_e}{\partial \dot{x}}\right|_{x_s,\dot{x}_s} [(\dot{x}-\dot{x}_e)-(\dot{x}_s-\dot{x}_e)]. \end{aligned} \tag{6}$$

Furthermore, x_s can be calculated by (4) at the steady-state as $f = k_e(x_s - x_e)^n$, which results in

$$x_s = x_e + \sqrt[n]{\frac{\bar{f}}{k_e}}. \tag{7}$$

Take $\dot{x}_s = 0$ and (4) into consideration, the partial derivative terms $\partial f_e/\partial x$ and $\partial f_e/\partial \dot{x}$ at $x_s, \dot{x}_s$ can be calculated as

$$\begin{aligned} \left.\frac{\partial f_e}{\partial x}\right|_{x_s,\dot{x}_s} =& nk_e(x_s-x_e)^{n-1} + nc_e(x_s-x_n)^{n-1}\dot{x}_s \\ =& nk_e(x_s-x_e)^{n-1} = nk_e(\frac{\bar{f}}{k_e})^{\frac{n-1}{n}} = \tilde{k}_e, \end{aligned} \tag{8}$$

$$\left.\frac{\partial f_e}{\partial \dot{x}}\right|_{x_s,\dot{x}_s} = c_e(x_s-x_e)^n = c_e\frac{\bar{f}}{k_e} = \tilde{c}_e. \tag{9}$$

By combining (8) and (9) with (6), we have

$$f_e(x,\dot{x}) = f_d + \tilde{k}_e(x-x_e) - \tilde{k}_e(x_s-x_e) + \tilde{c}_e\dot{x}. \tag{10}$$

Note that $\tilde{k}_e(x_s - x_e) = n\bar{f}$ holds after appropriate simplifications on (7) and (8), so the linearized HC model is

$$f_e = \tilde{k}_e(x-x_e) + \tilde{c}_e\dot{x} + (1-n)\bar{f}. \tag{11}$$

Hence, the dynamics for soft interaction with (3) becomes

$$\begin{aligned} m_i\ddot{e}_p + c_i\dot{e}_p + k_ie_p = & -k_f[\tilde{k}_e(x-x_e) \\ & + \tilde{c}_e\dot{x} + (1-n)\bar{f} - \bar{f}]. \end{aligned} \tag{12}$$

For the steady-state response, we have $\ddot{x}_d = 0$, $\dot{x}_d = 0$, $\ddot{x}_e = 0$, $\dot{x}_e = 0$, $\ddot{x} = 0$, and $\dot{x} = 0$. Hence, (12) becomes

$$k_ie_p = -k_f\tilde{k}_ee_p + k_f[n\bar{f} + \tilde{k}_e(x_e - \bar{x})]. \tag{13}$$

Thus, the steady-state position and force errors are

$$\begin{aligned} e_{pss} \approx & \frac{k_f}{k_i + k_f\tilde{k}_e}[n\bar{f} + \tilde{k}_e(x_e-\bar{x})] \\ e_{fss} \approx & -\frac{k_i}{k_f}e_{pss} = -\frac{k_i}{k_i + k_f\tilde{k}_e}[n\bar{f} + \tilde{k}_e(x_e-\bar{x})]. \end{aligned} \tag{14}$$

To achieve zero force error, one method is to track the generated virtual reference calculated by $\bar{x} = x_e + n\bar{f}/\tilde{k}_e$. It is evident that the parameters of HC model k_e, b_e, n, and the equilibrium position need to be known exactly. The complexity of the control system will increase significantly although the online identification of HC model has been proposed in [18], [29]. Moreover, there are still some limits that are posed on these methods. Alternatively, it can be observed that the zero force steady-state error can be achieved by setting $k_i = 0$ which avoids the need of HC model identification.

Remark 1. In this paper, the conditions of zero force tracking error are deduced based on the nonlinear HC model. Moreover, this study focus on the force tracking in a soft environment and hence $k_i = 0$ is chosen in this paper to simplify the controller implementation. Thus, the modified target impedance model is expressed as

$$m_i\ddot{e}_p + c_i\dot{e}_p = -k_fe_f, \tag{15}$$

which is employed in the following controller design.

IV. Robust Impedance Control Scheme

Fig. 3 shows the block diagram of the proposed impedance control scheme. It employs the impedance model as well as the adaptive control and sliding mode control techniques.

A. Impedance Error-based Auxiliary Variable

Based on (15), the impedance error is given by

$$\epsilon = m_i\ddot{e}_p + c_i\dot{e}_p + k_fe_f, \tag{16}$$

and an augmented impedance error is defined by

$$\bar{\epsilon} = \ddot{e}_p + C_i\dot{e}_p + K_fe_f, \tag{17}$$

where $C_i = \frac{c_i}{m_i}, K_f = \frac{k_f}{m_i}$.

By designing a new auxiliary variable z, (17) becomes

$$\bar{\epsilon} = \dot{z} + C_iz, \tag{18}$$

where the auxiliary variable z is given by $z = \dot{e}_p + e_l$, with the filtered force error defined as $\dot{e}_l + B_ie_l = K_fe_f$.

Therefore, $z \to 0$ will lead to $\epsilon \to 0$, and thus the control objective now is to minimize the auxiliary variable z.

B. Integral Backstepping Force Controller with Integral Terminal Sliding Function

To accommodate the unknown disturbance like friction and hysteresis in the USM-actuated end-effector, a sliding mode-based controller is developed. A novel integral terminal sliding manifold based on z is proposed to achieve finite-time convergence and better steady-state performance,

$$\sigma = \int [z + k_1\dot{z} + k_2\mathrm{sig}(z)^\rho]\,dt, \tag{19}$$

where $\mathrm{sig}(\cdot)^\rho = |\cdot|^\rho\mathrm{sign}(\cdot)$, $k_1 > 0$, $k_2 > 0$, and $1 < \rho < 2$.

Remarkably, the integral action is in corporated into the sliding function to improve the steady-state performance. This sliding function will converge in a finite time T_s, and

$$T_s \le \frac{k_1}{1-\rho}\ln\frac{|z(0)|^{1-\rho} + k_2}{k_2}, \tag{20}$$

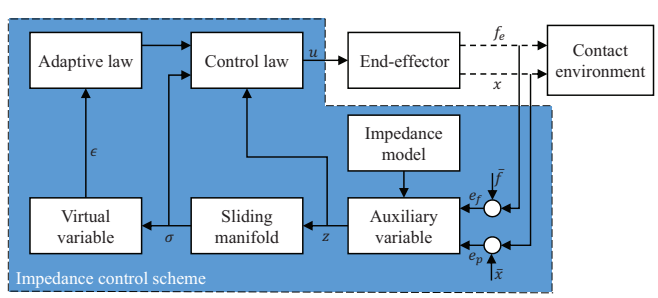

Fig. 3. Block diagram of the proposed impedance control scheme

where $z(0)$ is the initial value of z.

The time derivative of (19) is deduced as

$$\dot{\sigma} = k_1\dot{z} + z + k_2\text{sig}(z)^{\rho}. \tag{21}$$

Based on (19) and (21), the second-order auxiliary differential equations based on the integral terminal sliding mode surface is constructed as

$$\begin{aligned} \sigma_1 =& \sigma = \int [z + k_1\dot{z} + k_2\text{sig}(z)^{\rho}]\, dt,\ \dot{\sigma}_1 = \sigma_2 \\ \dot{\sigma}_2 =& \frac{d}{dt}[k_1\dot{z} + z + k_2\text{sig}(z)^{\rho}] \end{aligned} \tag{22}$$

Next, the backstepping method is employed to obtain the proposed control law. To improve the steady-state performance, the integral action is augmented in the control scheme. The integral error of σ_1 is defined as

$$\chi_1 = \int \sigma_1\, dt. \tag{23}$$

To drive the sliding function and its integration to zero, the Lyapunov function candidate V_1 is chosen as

$$V_1 = \frac{1}{2}\sigma_1^2 + \frac{\lambda_1}{2}\chi_1^2, \tag{24}$$

where λ_1 is a positive parameter. Then $\dot{V}_1$ is calculated as

$$\dot{V}_1 = \sigma_1\dot{\sigma}_1 + \lambda_1\chi_1\sigma_1 = \sigma_1\sigma_2 + \lambda_1\chi_1\sigma_1, \tag{25}$$

which can be rendered negative, i.e., $\dot{V}_1 < 0$ if we use ϕ as virtual signal defined by

$$\phi = \sigma_2^d = -\xi_1\sigma_1 - \lambda_1\chi_1, \tag{26}$$

where σ_2^d is the desired control force of σ_2, and ξ_1 is a positive parameter. The error between σ_2 and σ_2^d is given by

$$\varepsilon = \sigma_2 - \sigma_2^d = \sigma_2 - \phi, \tag{27}$$

and we can also obtain that

$$\sigma_2 = \varepsilon + \phi = -\xi_1\sigma_1 - \lambda_1\chi_1 + \varepsilon. \tag{28}$$

Take (28) into (25), yields

$$\dot{V}_1 = \sigma_1\sigma_2 + \lambda_1\chi_1\sigma_1 = -\xi_1\sigma_1^2 + \sigma_1\varepsilon. \tag{29}$$

Then, the integral error of ε is given by $\chi_2 = \int \varepsilon\, dt$.

To make the error ε and its integration χ_2 converge to zero, the following Lyapunov function is proposed,

$$V_2 = V_1 + \frac{1}{2}\varepsilon^2 + \frac{\lambda_2}{2}\chi_2^2, \tag{30}$$

where λ_2 is a position parameter. Then $\dot{V}_2$ is calculated as

$$\dot{V}_2 = -\xi_1\sigma_1^2 + \sigma_1\varepsilon + \lambda_2\chi_2\varepsilon + \varepsilon(\dot{\sigma}_2 - \dot{\phi}). \tag{31}$$

Theorem 1. *For the system* (2)*, the virtual variable z will converge to zero and achieve the target impedance* (15) *if the following control law and the integral terminal sliding function* (19) *are applied,*

$$\begin{aligned} u =& \frac{1}{b}[c_n\dot{x} + k_n x + f_e - \int \hat{K}_s\text{sign}(\varepsilon)\, dt] + \frac{m_n}{b}(\ddot{x}_d - \dot{e}_l) \\ & - \frac{m_n}{bk_1}[z + k_2\text{sig}(z)^{\rho} - \phi + \int (\sigma_1 + \xi_2\varepsilon + \lambda_2\chi_2)\, dt], \end{aligned} \tag{32}$$

with the update law

$$\dot{\hat{K}}_s = \gamma\frac{k_1}{m_n}|\varepsilon|, \tag{33}$$

where γ, ξ_2 are both positive parameters.

Proof of Theorem 1. The stability of the proposed controller is proven by the final Lyapunov function defined by

$$V_3 = V_2 + \frac{1}{2\gamma}\tilde{K}_s^2, \tag{34}$$

where $\tilde{K}_s = \hat{K}_s - K_s$ is the estimated error of K_s that is to update the upper bound of f_t, and K_s meets the condition $|K_s| > \Theta_{f_t}$. It is evident that (34) is continuous and non-negative, then $\dot{V}_3$ is given by

$$\dot{V}_3 = -\xi_1\sigma_1^2 + \sigma_1\varepsilon + \lambda_2\chi_2\varepsilon + \varepsilon(\dot{\sigma}_2 - \dot{\phi}) + \gamma^{-1}\tilde{K}_s\dot{\hat{K}}_s. \tag{35}$$

According to (22), we can obtain that

$$\dot{\sigma}_2 = \frac{d}{dt}[k_1(\ddot{x} - \ddot{x}_d + \dot{e}_l) + z + k_2\text{sig}(z)^{\rho}]. \tag{36}$$

Then, based on the model (2), it is calculated that

$$\ddot{x} = \frac{1}{m_n}(bu - c_n\dot{x}_n - kx - f_e - f_t). \tag{37}$$

Combine (35) and (37), it yields

$$\begin{aligned} \dot{\sigma}_2 =& \frac{d}{dt}[\frac{k_1}{m_n}(bu - c_n\dot{x} - k_n x - f_e - f_t) \\ & - k_1(\ddot{x}_d - \dot{e}_l) + z + k_2\text{sig}(z)^{\rho}]. \end{aligned} \tag{38}$$

By substituting (38) and (32) into (35), we have

$$\begin{aligned} \dot{V}_3 =& -\xi_1\sigma_1^2 - \xi_2\varepsilon^2 - \varepsilon\frac{k_1}{m_n}[\hat{K}_s\text{sign}(\varepsilon) + \dot{f}_t] \\ & + \gamma^{-1}(\hat{K}_s - K_s)\dot{\hat{K}}_s. \end{aligned} \tag{39}$$

Take the adaptive law (33) into consideration yields

$$\dot{V}_3 = -\xi_1\sigma_1^2 - \xi_2\varepsilon^2 - \frac{k_1}{m_n}(K_s|\varepsilon| + \dot{f}_t\varepsilon) < 0, \tag{40}$$

with $|K_s| > \Theta_{f_t}$. The above result demonstrates that σ and z will converge to zero in a finite time according to (20), and reach the desired impedance (15). The globally asymptotic stability is guaranteed by the backstepping method. □

C. Overall Control Law

To further avoid the estimated parameter $\hat{K}_s$ to be too big with the integral action in (33), a projection operator [30] is employed. With the lower and upper bounds of K_s, i,e, $K_{s,\max}$, and $K_{s,\min}$ the adaptive law is modified as

$$\dot{\hat{K}}_s = \text{Proj}_{\hat{K}_s}(\frac{\gamma}{m_n}|\sigma|), \tag{41}$$

where

$$\text{Proj}_{\hat{K}_s}(\cdot) = \begin{cases} 0, \text{ if } \hat{K}_s = K_{s,\max} \text{ and } \cdot > 0 \\ 0, \text{ if } \hat{K}_s = K_{s,\min} \text{ and } \cdot < 0 \\ \cdot, \text{ otherwise.} \end{cases}$$

Moreover, to simplify the controller implementation and avoid the derivative of signal, e_l can be calculated through filtering e_f by a transfer function $G_f(s)$ defined by

$$G_f(s) = \frac{K_f}{s + B_i}, \tag{42}$$

and $\dot{e}_l$ is obtained by $\dot{e}_l = K_f e_f - B_i e_l$.

Therefore, the overall control law is given by

$$\begin{aligned} u =& \frac{1}{b}[c_n\dot{x} + k_n x + f_e - \int \hat{K}_s \text{sign}(\varepsilon)\, dt] + \frac{m_n}{b} \\ & (\ddot{x}_d - K_f e_f + B_i e_l) - \frac{m_n}{bk_1}[z + k_2 \text{sig}(z)^\rho - \phi + \\ & \int (\sigma_1 + \xi_2 \varepsilon + \lambda_2 \chi_2)\, dt], \end{aligned} \tag{43}$$

with the adaptive law expressed by (41).

Remark 2. In this paper, an adaptive control law is also incorporated into the proposed control scheme to estimate the generally unknown upper bound of the total disturbance.

Remark 3. The proposed BCITSMC generates the control signal directly based on the impedance error. The extra inner-loop for position control to track the virtual position trajectory is not needed while using the proposed BCITSMC.

Remark 4. The control law (43) is deduced by setting $k_i = 0$ based on the analysis with the HC model so that precision force tracking can be achieved even in a soft environment.

V. Experiments, Results and Discussions

To verify the effectiveness of the proposed method, an experimental system setup is built as shown in Fig. 4. Besides the USM-actuated end-effector, a soft Polyethylene (PE) film is utilized as the soft object to be contacted. The overall impedance control scheme is implemented by the dSPACE DS-1104 control card with the sampling time of 1 ms.

A. Effects of Impedance Parameter k_i

To evaluate the effects of k_i, the references are set as 0.25Hz, 0.5 Hz, 1 Hz periodic S-curves with the tracking amplitude of 0.1 N, respectively. For the first condition, the impedance parameter is chosen as a fine-tuned $k_i = 3947.61$, and the second condition is with $k_i = 0$ based on the analysis in Section III. The results are performed during the soft interaction between the end-effector and one-layer soft membrane. The force tracking errors are plotted in Fig. 5 and the force root-mean-square error (RMSE, e_{rms}) is shown in Table I. It is obvious that both the two conditions can stabilize the interaction with the soft membrane. For the 0.25

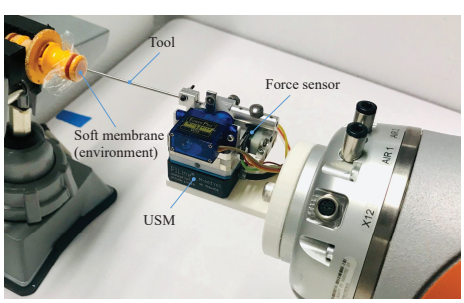

Fig. 4. Experimental system setup

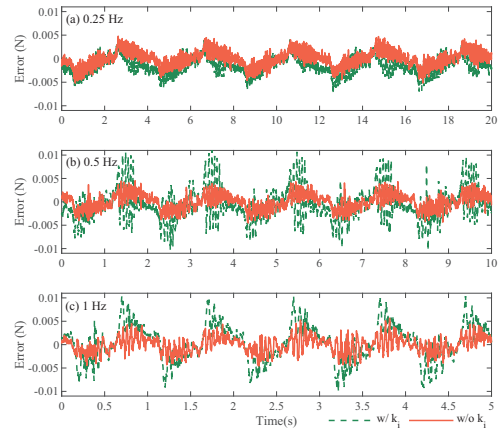

Fig. 5. Force tracking errors of the proposed controller with different k_i

TABLE I

RMSE of the proposed controller with different k_i

Statistical Errors (N)		0.25 Hz	0.5 Hz	1 Hz
with k_i	e_{rms}	0.0023	0.0033	0.0039
without k_i	e_{rms}	0.0016	0.0016	0.0017

Hz S-curve, the e_{rms} is 0.0023 N with k_i while it is 0.0016 N without k_i. As the frequency increases, the e_{rms} increases to 0.0039 N with k_i, and e_{rms} at 0.0017 N is achieved by the proposed method with $k_i = 0$. It should be noted that only the force tracking is concentrated and thus the zero fore error can be achieved by setting $k_i = 0$. In spite of that, the position of the USM is still constrained according to (14) due to the implementation of impedance model. The above results demonstrate that better force tracking performance can be achieved by the proposed BCITSMC with $k_i = 0$.

B. Comparative Results with Different Force Trajectories

To highlight the performance of the proposed control scheme, another three force tracking controllers are developed as benchmarks:

(i) Proportional-integral-derivative (PID)-based impedance control (PIDC): through the target impedance (3), a PID controller shown in (44) is designed to track the generated reference, similar to the method in [31],

$$u_p = -K_p e_p - K_i \int e_p\, dt - K_p \dot{e}_p. \tag{44}$$

(ii) Sliding mode-based impedance control (SMCC) [25],

$$\begin{aligned} u =& \frac{1}{b}[c_n\dot{x} + k_n x + f_e - k_s\sigma - d\text{sign}(\sigma)] + \frac{m_n}{b}(\ddot{x}_d - \dot{\xi}), \\ \sigma =& \dot{e}_p + \xi,\ \dot{\xi} = -\alpha\xi + k_p e_p + k_v \dot{e}_p + k_f e_f. \end{aligned} \tag{45}$$

(iii) Integral terminal sliding mode-based impedance control (ITSMC),

$$\begin{aligned} u =& \frac{1}{b}[c_n\dot{x} + k_n x + f_e - K_s\text{sign}(\sigma)] + \frac{m_n}{b}(\ddot{x}_d - \Lambda\dot{e}_p - \dot{e}_l) \\ & - \frac{m_n}{bk_1}[z + k_2 \text{sig}(z)^\rho], \end{aligned} \tag{46}$$

with the adaptive law (41).

Next, the tracking performance for the dynamic force is tested and compared. The references are set as 0.25 Hz, 0.5

Hz, 1 Hz periodic S-curves with the tracking amplitude of 0.1 N, respectively and one-layer soft membrane is used to verify the controller performance on tracking varying force. k_i is chosen as $k_i = 3947.61$ for PIDC and SMCC while k_i is set to zero for ITSMC and the proposed BCITSMC.

Table II lists the statistical results of the force tracking errors and Fig. 6 shows the comparative results of different controllers at different frequencies of 0.25 Hz, 0.5 Hz, 1 Hz.

For the lowest tracking speed at 0.25 Hz, PIDC and SMCC achieve the similar e_{rms}. However, the maximum absolute error (MaxAE) e_{max} of PIDC is smaller than the e_{max} of SMCC. Therefore, the performance of PIDC is better than that of SMCC. It should be noted that the largest error of PIDC occurs during rising phase of S-curve due to the limited position bandwidth of PID controller. On the contrary, the e_{max} of SMCC occurs when the S-curve is rising or falling because the impact of friction is significant. The variation of dynamic motion direction brings a suddenly changing disturbance to the system, but the SMCC cannot remove it effectively. For ITSMC, both the e_{rms} and e_{max} show that the performance is improved significantly by using the integral terminal sliding surface. Furthermore, with the proposed controller via backstepping technology, the e_{rms} and e_{max} improve 40.74% and 21.21%, respectively, in comparison with ITSMC.

For the 0.5 Hz S-curve shown in Fig. 6, although the e_{rms} of SMCC is smaller than that of PIDC, the e_{max} is still larger, which gets the same conclusion from the tracking results of 0.25 Hz S-curve. For ITSMC, the performance is nearly the same as 0.25 Hz S-curve. The performance of BCITSMC remains the best.

For the relatively high-frequency (i.e., 1 Hz) results, the performance of PIDC is the worst, and the steady-state force is only 0.088 N mainly due to its lower bandwidth. It can be concluded that PIDC cannot track high-speed trajectory. For SMCC, the error is large and the error caused by friction still exists. For the high-speed force tracking, the tracking error of ITSMC increases while the proposed controller remains the best performance with the similar e_{rms} and e_{max} even

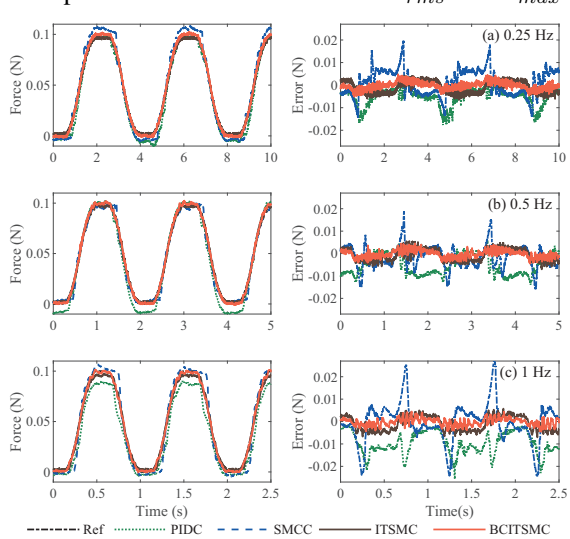

Fig. 6. Force tracking results of different S-curves with different controllers

TABLE II

FORCE TRACKING ERRORS FOR DIFFERENT TRAJECTORIES WITH DIFFERENT CONTROLLERS

Statistical Errors (N)		0.25 Hz	0.5 Hz	1 Hz
PIDC	e_{rms}	0.0063	0.0071	0.0108
	e_{max}	0.0181	0.0141	0.0257
SMCC	e_{rms}	0.0059	0.0053	0.0089
	e_{max}	0.0197	0.0199	0.0279
ITSMC	e_{rms}	0.0027	0.0027	0.0034
	e_{max}	0.0066	0.0071	0.0083
BCITSMC	e_{rms}	0.0016	0.0016	0.0017
	e_{max}	0.0052	0.0045	0.0057

at 1 Hz force tracking.

In summary, the employment of integral terminal sliding surface helps the system to obtain good tracking performance and the integration of backstepping technology further improves the performance effectively.

C. Results under Different Contact Environment

In the real application, the soft environment can be varying, for example, the human tissues are not identical from one to another. To evaluate the robustness of the proposed control scheme, the soft membranes with different layers are used in the experiments to simulate different soft contact environment. The reference is set as 0.5 Hz periodic S-curves with the amplitude of 0.1 N in the experiments.

Table III shows the force tracking errors when the soft membranes are with different layers (one-layer, two-layer and three-layer). As can be seen, although both errors increase as the number of layers increases, the amount of increase is very small Therefore, the above results show that the proposed control scheme is robust which is able to track the desired force under different soft environment precisely.

D. Results in Medical Application

To validate the effectiveness of the proposed control scheme in practical application, an experiment of a robot-

TABLE III

FORCE TRACKING ERRORS UNDER DIFFERENT SOFT ENVIRONMENT

Statistical Errors (N)		Layer 1	Layer 2	Layer 3
BCITSMC	e_{rms}	0.0016	0.0020	0.0023
	e_{max}	0.0045	0.0055	0.0058

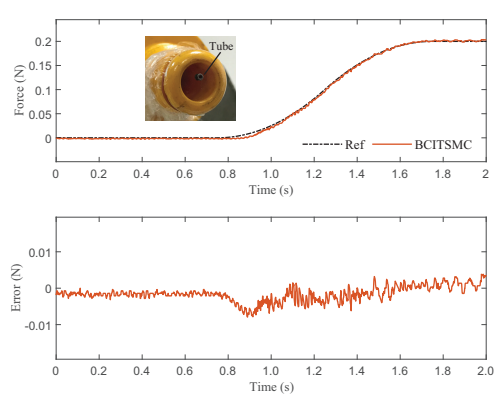

Fig. 7. Results of ear surgical operation

assisted ear surgical operation is conducted. In this experiment, the USM-actuated end-effector will carry out the automatic tube insertion on the soft film. Significantly, the first step is to contact the film gently and precisely, where a correct contact force can ensure the high success rate of the insertion. Fig. 7 shows the experimental results of this medical application. As can be seen, the contact force between the soft film and the tube is controlled precisely, which helps the end-effector insert the tube successfully on the thin and soft film.

VI. Conclusions

In this paper, BCITSMC, a novel robust impedance control scheme leveraging on backstepping technology and SMC was proposed and developed for an USM-actuated end-effector to achieve high precision force tracking in a soft environment. The HC nonlinear model was employed to investigate the impedance parameters on the steady-state performance during soft interaction. Furthermore, to facilitate the controller design, an auxiliary variable defined based on impedance error was constructed. The fast-convergence and accurate tracking performance of the desired reference were guaranteed by an integral-type terminal sliding manifold with the impedance error-based auxiliary variable. The robustness to the unknown disturbance was achieved by the integral backstepping approach and an adaptive law was designed to estimate the upper bound of the total disturbance. The overall control scheme was deduced by the Lyapunov theory with stability analysis. Finally, several experiments have been conducted which results showed that the proposed control scheme could achieve good force tracking performance as well as strong robustness in a soft environment.

References

[1] A. Billard and D. Kragic, "Trends and challenges in robot manipulation," *Science*, vol. 364, no. 6446, p. eaat8414, 2019.

[2] R. Li and H. Qiao, "A survey of methods and strategies for high-precision robotic grasping and assembly tasks — some new trends," *IEEE/ASME Trans. on Mechatronics*, vol. 24, no. 6, pp. 2718–2732, 2019.

[3] B. Komati, C. Clévy, and P. Lutz, "High bandwidth microgripper with integrated force sensors and position estimation for the grasp of multistiffness microcomponents," *IEEE/ASME Trans. on Mechatronics*, vol. 21, no. 4, pp. 2039–2049, 2016.

[4] H. B. Huang, D. Sun, J. K. Mills, and S. H. Cheng, "Robotic cell injection system with position and force control: Toward automatic batch biomanipulation," *IEEE Trans. on Robot.*, vol. 25, no. 3, pp. 727–737, 2009.

[5] K. K. Tan, W. Liang, L. P. Phuong, S. Huang, C. W. Gan, and H. Y. Lim, "Design of a surgical device for office-based myringotomy and grommet insertion for patients with otitis media with effusion," *J. of Med. Devices*, vol. 8, no. 3, 2014.

[6] Y. Li, K. P. Tee, R. Yan, W. L. Chan, and Y. Wu, "A framework of human–robot coordination based on game theory and policy iteration," *IEEE Trans. on Robot.*, vol. 32, no. 6, pp. 1408–1418, 2016.

[7] W. Liang and K. K. Tan, "Force feedback control assisted tympanostomy tube insertion," *IEEE Trans. on Control Syst. Technol.*, vol. 25, no. 3, pp. 1007–1018, 2016.

[8] W. Liang, J. Ma, and K. K. Tan, "Contact force control on soft membrane for an ear surgical device," *IEEE Trans. on Ind. Electron.*, vol. 65, no. 12, pp. 9593–9603, 2018.

[9] Y. Xie, D. Sun, C. Liu, H. Y. Tse, and S. H. Cheng, "A force control approach to a robot-assisted cell microinjection system," *The Int. J. of Robot. Res.*, vol. 29, no. 9, pp. 1222–1232, 2010.

[10] Z. Zarrouk, A. Chemori, and P. Poignet, "Adaptive force feedback control for 3d compensation of physiological motion in beating heart surgery," in *2010 IEEE/RSJ Int. Conf. on Intelligent Robots and Syst.* IEEE, 2010, pp. 1856–1861.

[11] J. Lee, M. Jin, N. Kashiri, D. G. Caldwell, and N. G. Tsagarakis, "Inversion-free force tracking control of piezoelectric actuatorsusing fast finite-time integral terminal sliding-mode," *Mechatronics*, vol. 57, pp. 39–50, 2019.

[12] N. Hogan, "Impedance control: An approach to manipulation: Part I theory," *J. of Dyn. Sys., Meas., Control*, vol. 107, no. 1, pp. 1–7, 1985.

[13] S. Jung, T. C. Hsia, and R. G. Bonitz, "Force tracking impedance control for robot manipulators with an unknown environment: theory, simulation, and experiment," *The Int. J. of Robot. Res.*, vol. 20, no. 9, pp. 765–774, 2001.

[14] B. Komati, C. Clévy, and P. Lutz, "Force tracking impedance control with unknown environment at the microscale," in *2014 IEEE Int. Conf. on Robot. and Automat. (ICRA)*. IEEE, 2014, pp. 5203–5208.

[15] J. Duan, Y. Gan, M. Chen, and X. Dai, "Adaptive variable impedance control for dynamic contact force tracking in uncertain environment," *Robot. and Auton. Syst.*, vol. 102, pp. 54–65, 2018.

[16] L. Cheng, Z.-C. Zhu, G. Shen, S. Wang, X. Li, and Y. Tang, "Real-time force tracking control of an electro-hydraulic system using a novel robust adaptive sliding mode controller," *IEEE Access*, 2019.

[17] S. Khadraoui, M. Rakotondrabe, and P. Lutz, "Interval force/position modeling and control of a microgripper composed of two collaborative piezoelectric actuators and its automation," *Int. J. of Control, Automat. and Syst.*, vol. 12, no. 2, pp. 358–371, 2014.

[18] R. Schindeler and K. Hashtrudi-Zaad, "Online identification of environment hunt–crossley models using polynomial linearization," *IEEE Trans. on Robot.*, vol. 34, no. 2, pp. 447–458, 2018.

[19] C. Yang, Y. Xie, S. Liu, and D. Sun, "Force modeling, identification, and feedback control of robot-assisted needle insertion: a survey of the literature," *Sensors*, vol. 18, no. 2, p. 561, 2018.

[20] C. Ng, W. Liang, C. W. Gan, H. Y. Lim, and K. K. Tan, "Optimization of the penetrative path during grommet insertion in a robotic ear surgery," *Mechatronics*, vol. 60, pp. 1–14, 2019.

[21] A. Pappalardo, A. Albakri, C. Liu, L. Bascetta, E. De Momi, and P. Poignet, "Hunt–crossley model based force control for minimally invasive robotic surgery," *Biomed. Signal Process. and Control*, vol. 29, pp. 31–43, 2016.

[22] W. Liang, J. Ma, C. Ng, Q. Ren, S. Huang, and K. K. Tan, "Optimal and intelligent motion control scheme for an ultrasonic-motor-driven xy stage," *Mechatronics*, vol. 59, pp. 127–139, 2019.

[23] J. Y. Lau, W. Liang, and K. K. Tan, "Adaptive sliding mode enhanced disturbance observer-based control of surgical device," *ISA Trans.*, vol. 90, pp. 178–188, 2019.

[24] Q. Xu and M. Jia, "Model reference adaptive control with perturbation estimation for a micropositioning system," *IEEE Trans. on Control Sys. Technol.*, vol. 22, no. 1, pp. 352–359, 2013.

[25] H. C. Liaw and B. Shirinzadeh, "Robust generalised impedance control of piezo-actuated flexure-based four-bar mechanisms for micro/nano manipulation," *Sensors and Actuators A: Physical*, vol. 148, no. 2, pp. 443–453, 2008.

[26] K. Kiong Tan, W. Liang, S. Huang, L. P. Pham, S. Chen, C. Wee Gan, and H. Yee Lim, "Precision control of piezoelectric ultrasonic motor for myringotomy with tube insertion," *J. of Dyn. Syst., Meas., Control*, vol. 137, no. 6, 2015.

[27] Z. Feng, J. Ling, M. Ming, W. Liang, K. K. Tan, and X. Xiao, "Signal-transformation-based repetitive control of spiral trajectory for piezoelectric nanopositioning stages," *IEEE/ASME Trans. on Mechatronics*, vol. 25, no. 3, pp. 1634–1645, 2020.

[28] Z. Feng, W. Liang, J. Ling, X. Xiao, K. K. Tan, and T. H. Lee, "Integral terminal sliding-mode-based adaptive integral backstepping control for precision motion of a piezoelectric ultrasonic motor," *Mech. Syst. and Signal Process.*, vol. 144, p. 106856, 2020.

[29] A. Haddadi and K. Hashtrudi-Zaad, "Real-time identification of hunt–crossley dynamic models of contact environments," *IEEE Trans. on Robot.*, vol. 28, no. 3, pp. 555–566, 2012.

[30] S. Bashash and N. Jalili, "Robust adaptive control of coupled parallel piezo-flexural nanopositioning stages," *IEEE/ASME Trans. on Mechatronics*, vol. 14, no. 1, pp. 11–20, 2009.

[31] J. Y. Lau, W. Liang, and K. K. Tan, "Enhanced robust impedance control of a constrained piezoelectric actuator-based surgical device," *Sensors and Actuators A: Physical*, vol. 290, pp. 97–106, 2019.